Journal of Applied Fluid Mechanics, Vol. 16, No. 10, pp. 1901-1915, 2023.
Available online at www.jafmonline.net, ISSN 1735-3572, EISSN 1735-3645.
https://doi.org/10.47176/jafm.16.10.1889

Suppressing Methods of the Pressure Fluctuation in Open Jet Wind Tunnels

H. Xingjun, L. Yufei, S. Keyuan, G. Peng† and W. Jingyu

State Key Laboratory of Automotive Simulation and Control, Jilin University, Changchun 130022, China

†*Corresponding Author Email: gp323@jlu.edu.cn*

ABSTRACT

Due to the distinctive structure of the test section, the open jet wind tunnel generates low-frequency pressure fluctuations (LFFs) within the range of typical wind speeds. These fluctuations significantly compromise the quality of the flow field in the test section. The evolution of the flow structure and vortex is analysed through the improved delayed detached eddy simulations (IDDES). The LFFs and the control mechanism in the open jet wind tunnel of Jilin University are then studied. The interaction between the large-scale vortex shedding at the nozzle exit and the collector forms the edge feedback, which is the main reason for the pressure fluctuation. According to the feedback mechanism, the LFFs are suppressed using the throat gap and by improving the collector shapes. The results show that the increase of the throat gap length at the collector can significantly alleviate the pressure accumulation inside the collector. The change of the collector shapes can control the impact area and time of the incoming flow, or produce permanent vortex structure to affect the impact shape of the vortex and the flow field at the collector, which allows to control the LFFs. This study lays a solid foundation for further comprehension of the aerodynamic characteristics of the open jet wind tunnels.

Article History
Received April 16, 2023
Revised June 9, 2023
Accepted June 20, 2023
Available online July 29, 2023

Keywords:
Pressure fluctuation
Wind tunnel
Convective instability
Detached eddy simulation
Jet shear layer
Aerodynamics

1. INTRODUCTION

With the development of the automobile industry and the continuous improvement of the driving speed, automobile aerodynamics has been widely studied, and the automobile wind tunnels are indispensable test facilities to evaluate and measure the vehicle aerodynamic characteristics (Liu, 2005). The automobile wind tunnel can reproduce the driving process and environmental changes, so as to obtain the aerodynamic characteristics, acoustic characteristics, heat dissipation of various components, and adaptability to the climate and environment of the vehicle (Taketo, 1989; Fu, 1998; Barlow et al., 1999). This paper aims at studying a three-quarter return flow wind tunnel, which is considered as the main means of automobile aerodynamic test and holds immense importance in the product design and development phase. However, the jet from the nozzle produces a larger vortex structure and vortex shedding at a certain frequency in the shear layer.

The LFFs in open jet wind tunnels originate from the special core area structure (Hu et al., 2022). According to the Kelvin–Helmholtz instability mechanism, the jet flows from the nozzle into the stable flow field and an unstable velocity section is found between the jet injection and ambient fluid. The continuous fluid with shear velocity is vulnerable to instability due to the small disturbances that result in vortices. According to the acoustic–vortex coupling mechanism (Flandro & Jacobs, 1973), vortex shedding causes jet tone. If the excitation matches with the acoustic mode of the test section or the circuit of the wind tunnel, it will cause strong periodic fluctuations in the whole field. These fluctuations are known as low-frequency pressure fluctuations (LFF) with a frequency below 20 Hz (Zheng et al., 2007), and they disturb the space-time uniformity of the core area field, pose a threat to the tunnel structure's safety, and impact the experimental outcomes' accuracy (Thomas, 2016; Duell et al., 2002).

In 1871, the world's first wind tunnel was built in Greenwich, England, in order to obtain the aerodynamic drag of the measured object (Li, 2015). The American Aerospace Society then defined the wedge feedback effect through a study of the interaction between the

NOMENCLATURE

AAWT	Aeroacoustic Wind Tunnel		
CFD	Computational Fluid Dynamics	LLM	Logarithmic-Layer Mismatch
Cp	pressure fluctuation coefficient	p'	static pressure fluctuation level, Pa
Cp_{rms}	root mean square value of the pressure fluctuation coefficient	PIV	Particle Image Velocimetry
DDES	Delayed Detached Eddy Simulation	q_∞	freestream dynamic pressure, Pa
DES	Detached Eddy Simulation	Q	second invariant of the velocity gradient tensor, /s^2
dt	time step, s	RANS	Reynolds-Averaged Navier–Stokes
G	width of the gap, mm	S	antisymmetric tensor of the velocity gradient, /s
HAWT	Hyundai Aeroacoustic Wind Tunnel	SPL	Sound Pressure Level
IDDES	Improved Delayed Detached Eddy Simulation	T_f	period of the pressure fluctuation, s
LES	Large Eddy Simulation		
LFF	Low-Frequency Pressure Fluctuation	Ω	symmetric tensor of the velocity gradient, /s

nozzle exits and the collectors, which indicates the pressure fluctuation phenomenon in the wind tunnel caused by the free jet structure near the nozzle (Ahuja et al., 1997; Soderman & Olson, 1992). Manuel (1992) conducted an experiment to change the structure of the collector. He deduced that the fluctuation phenomenon of the collector with bell mouth shape was the most obvious, and the straight plate structure at a certain angle to the incoming flow was better. Lacey (2004) used a triangular collector structure in a scale wind tunnel to effectively reduce the pressure fluctuations.

Many wind tunnels suffer from LFFs upon first use. The vibrations in the first calibration phase of the German–Dutch wind tunnels in 1981 reached levels that are critical for the test hall structure, which is due to the LFFs generated by the open jet (Holthusen & Kooi, 1997). Sellers et al. (1985) studied the flow fluctuations in the 4 m × 7 m Langley tunnel. Wiedemann et al. (1993) assessed the AUDI aeroacoustic wind tunnel during its early design stage to prevent shear layer impingement on the collector that could cause discrete-frequency open jet excitations. The Hyundai aeroacoustic wind tunnel (HAWT) pressure fluctuations were determined during the improvement of its three-fourth open jet test section. The edgetone–feedback from the nozzle to the collector excited the acoustic mode of the entire wind tunnel circuit (Rennie et al., 2004). Kudo et al. (2009) demonstrated that the acoustic modal frequency of the whole circuit and the feedback frequency of the edgetone are mutually locked. In fact, this is the most critical factor for LFFs. In 2010, four areas of significant oscillations occurred in a full-scale S2A wind tunnel at wind velocities ranging between 10 m/s and 60 m/s (Amandolese & Vartanian, 2010). In the same year, the new BMW Aerodynamisches Versuchszentrum wind tunnel center (Duell et al., 2010) reported the open jet LFF phenomenon. In addition, the Helmholtz resonator was used and tuned to the selected low frequency in order to improve the pressure fluctuation coefficient. The Energy and Environment Test Center (Bender et al., 2011) (i.e., the new BMW Climatic Testing Complex) demonstrated satisfactory performance of the pressure fluctuation coefficient in the full wind speed range. The results of the scale model wind tunnel of Mitsubishi Heavy Industries' R & D center showed that the wind speed is proportional to the fluctuating frequency, while the circuit length is inversely proportional to it. The obtained results were applied to the design and construction of Toyota's full-size aeroacoustic wind tunnel (Tadakuma et al., 2014). Blumrich et al. (2015) developed a new optimized vortex generator during the latest technical upgrading and reconstruction of the full-size aeroacoustic wind tunnel at the University of Stuttgart. This generator plays a significant role in restraining the fluctuation phenomenon.

With the advancements in the Computational Fluid Dynamics (CFD) simulation technology, more researchers applied numerical methods to evaluate and optimize the performance of wind tunnel components (Ghani et al., 2001; Doolan & Morgans 2007; Abdelhamed et al. 2014; Kesharwani *et al*. 2017; Qu et al. 2018; Zanoun, 2018). The DaimlerChrysler full-scale vehicle Aeroacoustic Wind Tunnel (AAWT) employed CFD and various scale-model experimentsl to optimize its performance in terms of excellent flow quality and low background noise during its design and commissioning processes (Walter et al. 2003). Calautit and Hughes (2016) also provided a set of theoretical and computational methods that can be used to calculate closed-circuit wind tunnel models, which can improve the prediction accuracy when performing CFD of wind

tunnels. Their wind tunnel model includes many details, such as 90° guide vanes at the corners and horizontal and vertical diffuser splitting plates, which help improve the uniformity of the flow field in the test section. Li et al. (2009) and Yang and Zhao (2017) applied simulation and experimental methods to the design of aeroacoustic wind tunnels, while analyzing and comparing the application of corner deflector flow losses and different turbulence models in corner simulation calculations. An in-depth study was then conducted on the impacts of different diffusion angles, collector shapes, collector angles, and nozzle and collector sizes on the axial static pressure gradient in the test section. Improvement methods were also proposed, providing a reference for the theory and design of wind tunnel related components (Li et al., 2010, 2014; Xu et al., 2014; Li et al., 2017). In the study process of the FL-14 wind tunnel, Jin et al. (2014) focused on the unsteady RANS simulation of the impact of the opening and closing of the collector through-hole on the pressure fluctuation. They deduced that the existence of through-holes can effectively suppress the fluctuation phenomenon. Kesharwani et al. (2017) simulated and optimized the number of blades and structural form of the axial flow fan in the power section, which allows to reduce the background noise of the fan and to improve its pressure efficiency. Jia et al. (2019) simulated the vortex shedding structure in the shear layer of the jet at the nozzle using the large eddy simulation (LES) method. Their findings closely matched the results of the Particle Image Velocimetry (PIV) tests, and may serve as a reference for further numerical simulation studies on fluctuations.

Due to the lack of understanding of the LFFs in wind tunnels, the traditional studies are mostly limited to the application of a single suppression measure. For the sake of economic cost, most experiments are conducted on scale models. In practical applications with reconstruction requirements of large wind tunnels, only the elimination of the LFFs is given priority. However, the mechanism of this phenomenon is not deeply analyzed and explored. At present, there are few full scale and full loop digital model simulation schemes for the numerical exploration of wind tunnels. At present, there are limited studies available on how to control the general phenomenon of LFFs during the design phase of open jet wind tunnels. The results that have been obtained thus far are limited to providing only a preliminary explanation of the fluctuation phenomenon. Effectively avoiding LFFs and achieving satisfactory flow field quality across the full range of wind speeds are significant challenges that open jet wind tunnels must overcome. This study adopts the IDDES technology to reconstruct flow field information in an open jet and return flow wind tunnel. The computation results are compared with experimental ones. The fluctuation phenomenon is suppressed from the improvement of throat gaps and collector shapes according to the feedback mechanism. This study provides a theoretical support for the in-depth understanding of the LFF characteristics of open jet wind tunnels.

2. NUMERICAL METHOD AND THE SIMPLIFIED MODEL

2.1 Numerical Method

The unsteady 3D compressible Navier–Stokes equations are solved in inertial coordinates using the Star CCM+2020 commercial finite volume solver. The equations are closed with the perfect gas law defined as:

$$\rho = \frac{Mp}{R_u T} \tag{1}$$

where ρ is the density, M is the molecular weight, p is the pressure, T is the temperature, and $R_u = 8314.4621$ J/kmol K is the universal gas constant.

In this study, the improved delayed detached eddy simulations (IDDES) are employed in all the computations. Menter and Kuntz (2004) implemented the capacity of the Delayed Detached Eddy Simulations (DDES) which uses the Reynolds-averaged Navier–Stokes (RANS) equation in areas near the wall and large eddy simulation (LES) in areas outside the boundary layer. IDDES is an enhanced version of the original Detached Eddy Simulation (DES) method, which successfully solves the logarithmic-layer mismatch (LLM) problem (Nikitin & Nicoud, 2000) and aims to mitigate the impact of grid-induced separation arising from inadequate activation of LES in the near-wall zone. It merges the DDES and wall-modeled LES approaches and modifies the dissipation rate scale of the turbulent kinetic energy transport equation of the SST $k-\omega$ model (Gritskevich et al., 2012). The IDDES employs a novel subgrid length scale definition that accounts for the distance from the wall. The grid filter formula is expressed by:

$$\Delta = \min\left[\max\left(C_w d_w; C_w h_{max}; h_{wn}\right); h_{max}\right] \tag{2}$$

where $C_w = 0.15$ is an empirical constant, h_{max} is the maximum value of grid spacing in all the three directions, and h_{wn} is the grid spacing in the normal direction of the wall.

The length scale of LES and URANS is given by:

$$l_{IDDES} = \overline{f_d}\left(1+f_e\right)l_{URANS} + \left(1-\overline{f_d}\right)l_{LES} \tag{3}$$

$$l_{\mathrm{URANs}} = \sqrt{\mathrm{k}}/0.09\omega \tag{4}$$

$$l_{LES} = C_{DES}\Delta \tag{5}$$

where $\overline{f_d}$ is a blending function between the URANS and the LES and f_e is the boosting function added in the definition of the length scale. Convective fluxes are approximated with an 85% bounded central difference and 15% second-order upwind scheme. Time integration is achieved using the second-order accurate three-level time Euler scheme with a time step (dt) of 0.01s. Pressure-velocity coupling is done via the SIMPLE algorithm. Solid and adiabatic wall conditions are imposed

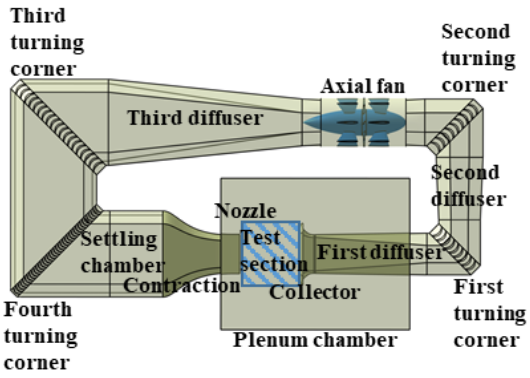

Fig. 1 Top view of the wind tunnel

throughout the wind tunnel. In the power section, the sliding grid method is used to simulate the drive of the actual fan rotation to the fluid in the wind tunnel circuit and the supplement of the fan to the fluid energy loss at a constant wind speed. The steady-state simulation results serve as the initial flow field conditions for all the IDDESs, providing high-precision flow field information for the initiation and flow separation under inverse pressure gradients. After an initial 50 seconds, the flow in the simulation is sampled for 10 seconds to ensure accuracy. The frequency resolution satisfies the Nyquist sampling theorem, which is consistent with the Hu et al. (2022).

2.2 Wind Tunnel Model

Jilin University's automobile wind tunnel is an open jet, low-speed, and return-flow wind tunnel, as illustrated in Fig. 1. The wind tunnel is situated in a testing hall and is mounted on the ground using brackets, with the control room located on the test section side. Sound source propagation is minimized using glass and sound-absorbing materials, along with rectification devices such as honeycombs and damping nets. The test space measures 8 m in length, 4 m in width, and 2.2 m in height, with a maximum speed of 60 m/s to accommodate a wide range of applications. The nozzle has a rectangular cross-section and an equivalent hydraulic diameter of 2.93 m. The lengths of the circuit, long, and short axes are 114, 43, and 14 m, respectively. The shrinkage and diffusion ratios are 5.17 and 1.84, respectively.

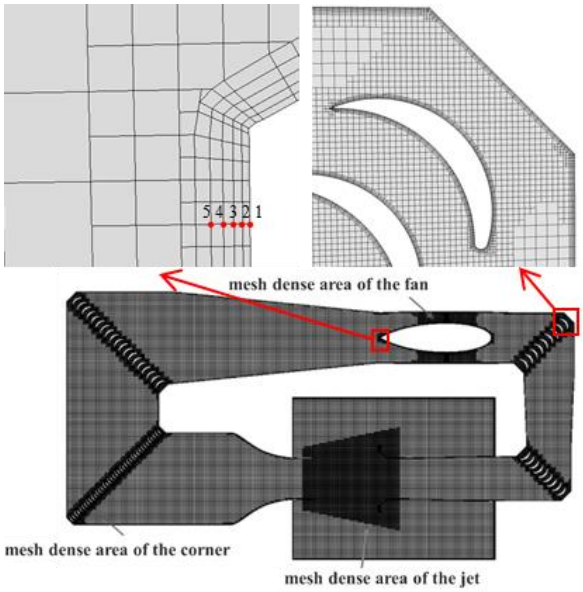

Fig. 2 The mesh on the central plane located at z=0

The computational domain is discretized with the trimmed cell mesher. The numerical accuracy is determined by performing simulations based on meshes with different sizes for the wind tunnel model. A slice of the mesh is shown in Fig. 2. The computational cells are dense in the corner of each wind tunnel, the fan is in the power section, and the jet area of the focused test section is where the flow change is violent. The flow near the wall is simulated with a five-layer transition from the normal direction of the wall grid.

The spatial resolutions of the eight grids are presented in Table 1. The monitored datum is the average wind speed in the axial cross section where the nozzle anemometer is located. The solution settings of all the examples are consistent. The volume grid size and space growth rate in densified areas, such as the flow channel, corner, and test section of the tunnel, are modified only in accordance with the flow field structure characteristics in the computational domain. The volume grid space growth rate is defined as the rate at which the cell size increases from one size to another within the trimmed cell. The growth rate defines the transformation of the cell size by specifying the minimum number of cell layers for each size.

Table 1 Details of the grids

Grid	Volume grid size in the densified areas (mm)	Volume grid space growth rate	Number of grids ($\times 10^7$)	LFF	Fluctuation frequency (Hz)
Grid1	160	1	0.95	no exist	-
Grid2	160	2	1.12	no exist	-
Grid3	160	4	1.29	weak	-
Base0	80	2	1.40	exist	2.7
Grid4	80	4	1.68	exist	2.7
Grid5	80	8	2.10	exist	2.7
Grid6	40	2	2.60	exist	2.8
Grid7	20	2	5.20	exist	2.7

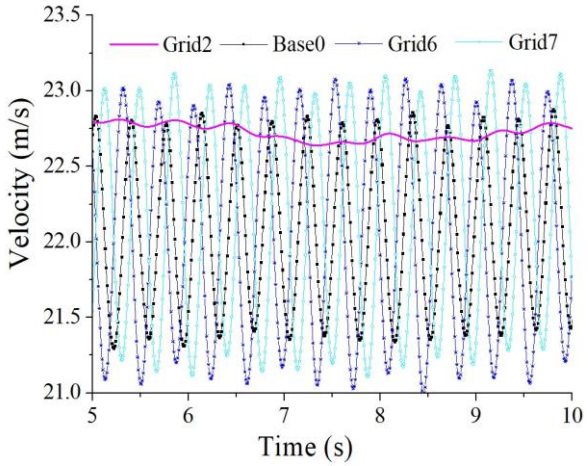

Fig. 3 Influence of the volume grid size in the densified areas on simulation results

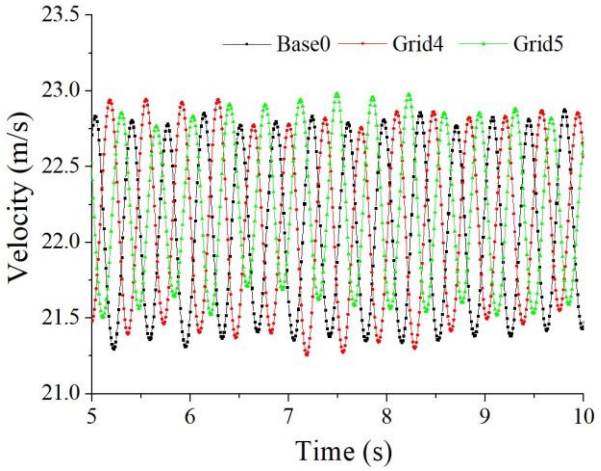

Fig. 4 Influence of the volume grid space growth rate on simulation results

For example, a growth rate of 2 indicates that at least two equally sized cell layers are converted each time. The results showed that the area where the nozzle, test section, and collector form boundary conditions for the jet flow should be densified with the number of grids. The number of grids in the launching basin exerts a significant effect on the simulation of the fluctuation phenomenon, as illustrated in Fig. 3. The grid density at the wind tunnel circuit, power section, and corner deflector is appropriate when the number of flow field grids in the test section is fixed. Moreover, the effect on the fluctuation phenomenon is insignificant, as shown in Fig. 4. Using the grid division strategy, the fluctuation of the wind speed with time (Fig. 4) and the fluctuation frequency (Table 1) show that the frequency is basically the same although the amplitude is slightly different when the fluctuation phenomenon at the nozzle of the test section is formed and remains stable. This indicates that the grid density no longer exerts a significant effect on the fluctuation frequency when the sequential vortex shedding in the jet shear layer and its primary structure can be captured by numerical simulation. This study finally adopts the grid scheme of Base0 which contains cells.

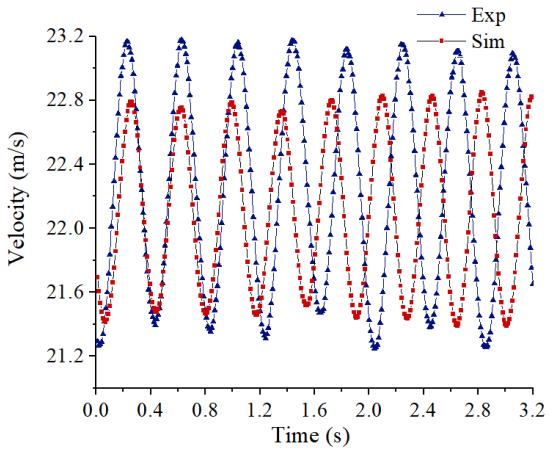

(a) Velocity fluctuation in the time domain

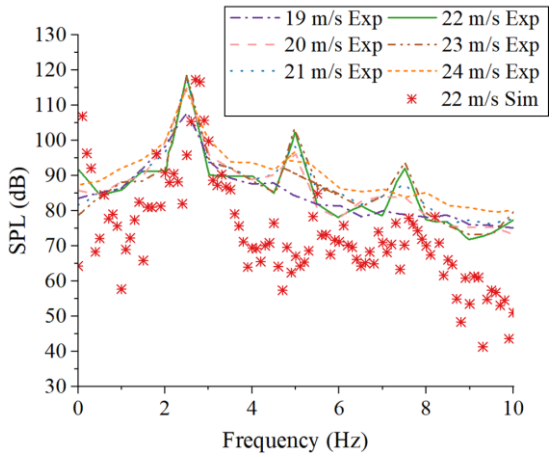

(b) Sound pressure level in the frequency domain

Fig. 5 Comparison between simulation and experimental results

Table 2 The characteristic parameters

Model	Frequency (Hz)	C_p	SPL (dB)
Simulation	2.7	0.046	116.7
Experiment	2.5	0.049	118.0

2.3 Validation of the Present Computation

Figure 5 presents a comparison between the simulation and experimental results. The characteristic parameters are shown in Table 2. The experiment is conducted in the automobile wind tunnel of Jilin University. The specific experimental equipment and process are consistent with the description presented in the study of Hu *et al*. (2022). *Cp* is a coefficient used to measure the level of the pressure fluctuation of a flow field that experiences large transient changes. Typically, the root mean square value of the pressure fluctuation coefficient (Cp_{rms}) is used to describe the LFFs (Reshotko et al., 1997; Saric & Reshotko 1998; Owen & Owen, 2008). *Cp* is expressed as:

$$Cp = \frac{p'}{q_\infty} \tag{8}$$

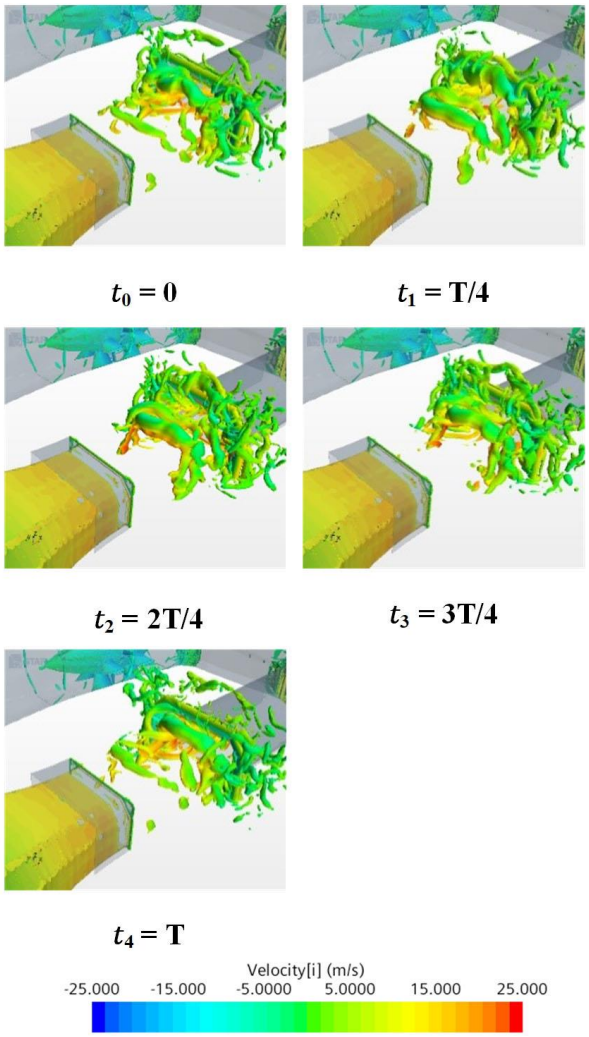

Fig. 6 Vortex rings formed in the jet shear layer

where p' is the static pressure fluctuation level (Pa).

q_∞ is the freestream dynamic pressure (Pa).

The simulation and experimental results show strong pressure fluctuation at 22 m/s, with a Reynolds number equal to 4.2×10^6. The dominant peak frequencies in the computation and experiment are 2.7 Hz and 2.5 Hz, respectively. The computation accurately predicts the most dominant frequency observed in the experiment. The computation and experiment show that there are three peak values of the Sound Pressure Level (SPL) in the frequency domain, and there is a multiple relationship between the frequencies corresponding to the peak values. This indicates that the trends between the computation and experimental results are consistent. The SPL amplitude difference in the computation and experimental results is approximately 1.3 dB.

Figure 6 shows the vortical structures visualized by the iso-surfaces of the second invariant of the velocity gradient tensor $Q = 200/s^2$ while the flow velocity is attached to the iso-surface for a period T_f. Q is expressed as:

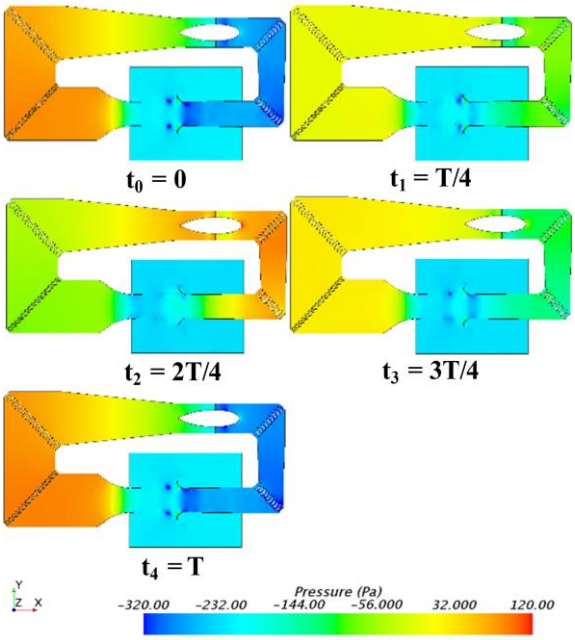

Fig. 7 Pressure in XY plane

$$Q = \frac{1}{2}\left(\|\Omega\|_F^2 - \|S\|_F^2\right) \tag{9}$$

where Ω is the symmetric tensor of the velocity gradient and S is the antisymmetric tensor of the velocity gradient.

Figure 6 illustrates the emergence of vortex rings in the shear layer of the jet. These rings travel down the stream and collide with the collector, breaking up into several smaller, disordered vortex structures. Meanwhile, an additional vortex ring is generated upstream near the nozzle exit and gradually evolving. The cycle is repeated due to periodic changes in pressure and mass flow rates. Since the nozzle has a rectangular cross-section, the curling behavior of the vortices varies along the long and short sides, with the shorter-side vortices exhibiting faster movement in the direction of flow. Consequently, the long-side vortices manifest in an inverted V-shape, connecting to the shorter-side vortices.

Figure 7 shows the pressure change in one cycle. The connection between the collector and the diffusion section at t_0 is in the maximum negative pressure status, with small and strong low pressure regions exist. From the test section to the diffuser, the pressure distribution displays a "low-high-low" pattern. The large pressure differential causes the flow field to be the most blocked state during this period. The intensity of the vortex decreases and the positive pressure region of the collector decreases at t_1 after the tail vortex collides with the collector. The tail vortex breaks up and escapes outward at t_2. The vortices on both sides of the nozzle smoothly develop and the flow field at the collector relatively calm at t_3. The intensity of the vortices on both sides reaches a large value and the flow field returns to t_0 at t_4. The pressure wave propagates a full loop within one cycle, traveling at the speed close to the sound velocity. There is a jump in pressure before and after the fan, which is mainly attributed to the power

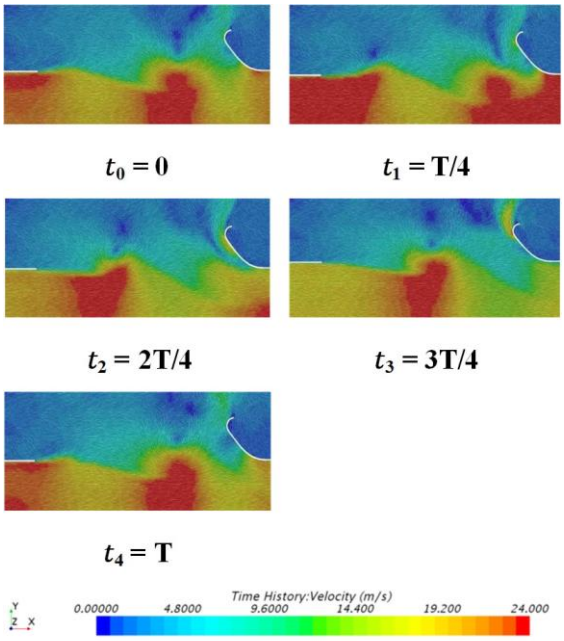

Fig. 8 Velocity vector in XY plane

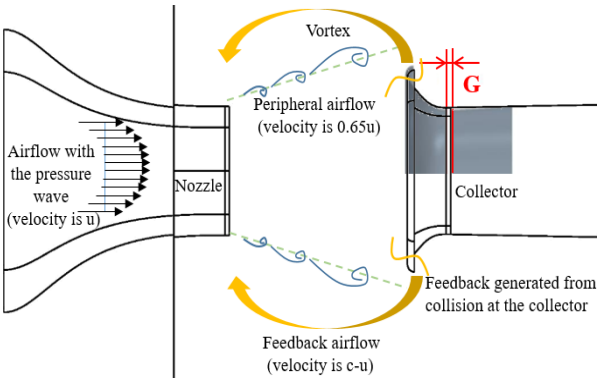

Fig. 9 Edge feedback and throat gap at the collector

source in the power section that supplements the pressure energy. Figure 8 shows the velocity vector fields in the XY plane with a texture-based technique referred to as line integral convolution (Cabral & Leedom, 1993), which involves convoluting a white noise image along streamlines computed from the vector field. It can be seen that the violent oscillations of the jet shear layer in a period and the strong flow exchange between the core flow field area and the periphery of the test section open and close the shear layer at certain times. The flow field in the rear section of the test area is significantly disturbed because of the invasion of the external flow field. Hence, the flow field parameters, such as the velocity and pressure, violently oscillate and cause fluctuation.

3. THROAT GAPS AT COLLECTORS

The collector is an important part of the edge feedback. The vortex ring affects the collector and breaks when the air flow generated at the nozzle exit moves to the rear section of the test section. In addition, the pressure wave

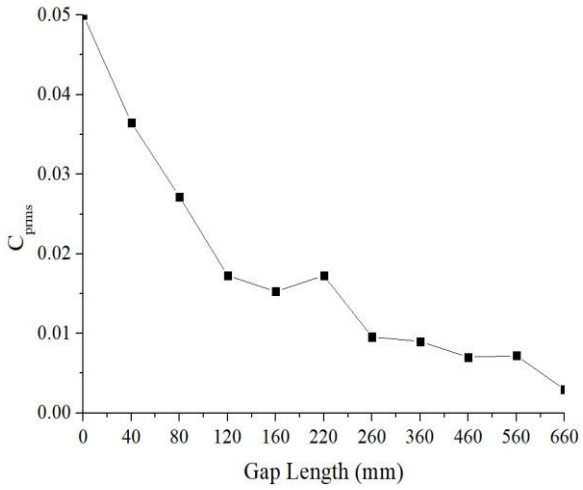

Fig. 10 Fluctuation within the range of 0-660mm

reversely formed induces the new vortex generation at the nozzle, as shown in Fig. 9. At t_0, a large negative pressure area exists at the connection between the collector and the diffusion section, as shown in Fig. 7. The negative pressure region, together with the low pressure of the vortex and the positive pressure on the windward side of the collector, plays a blocking role in the pressure fluctuation cycle. The gap created at the connection of the collector and the diffusion section can alleviate the pressure fluctuation in the fluctuation cycle. The influence of the length of the throat gap on the pressure fluctuation is also studied.

The throat gap generated at the collector is illustrated in Fig. 9. The gap with a width of G mm is the junction of the collector and the diffusion section, where the junction point is the starting position of the throat gap which extends backward. The basic example of G = 160 mm is denoted by g160. This value is the existing design size of the real wind tunnel at this location.

Figure 10 shows the fluctuation within the range of 0–660 mm. The throat gaps can alleviate the pressure fluctuation of the circuit, and their control effect provides regularity to a certain extent. The nine groups can be roughly divided into three stages according to the damping effect. 1) Linear stage. The length of the throat gap is in the range of 0–120 mm, and Cp_{rms} decreases approximately linearly with the increase of the length. 2) Stable stage. Cp_{rms} basically remains unchanged with the increase of the gap length in the range of 120–220 mm, and the same range is 260–560 mm. Note that in this stage, Cp_{rms} is insensitive to the gap length. 3) Mutation stage. Cp_{rms} rapidly decreases with the increase of the gap length in the ranges of 220–260 mm and 560–660 mm.

Figure 11 shows Lambda 2 under two conditions. The existence of the throat gap generates a new vortex containing high energy at the most chocking moment in the gap. These small flow structures are staggered from the large eddy fluctuations in the core flow field. The

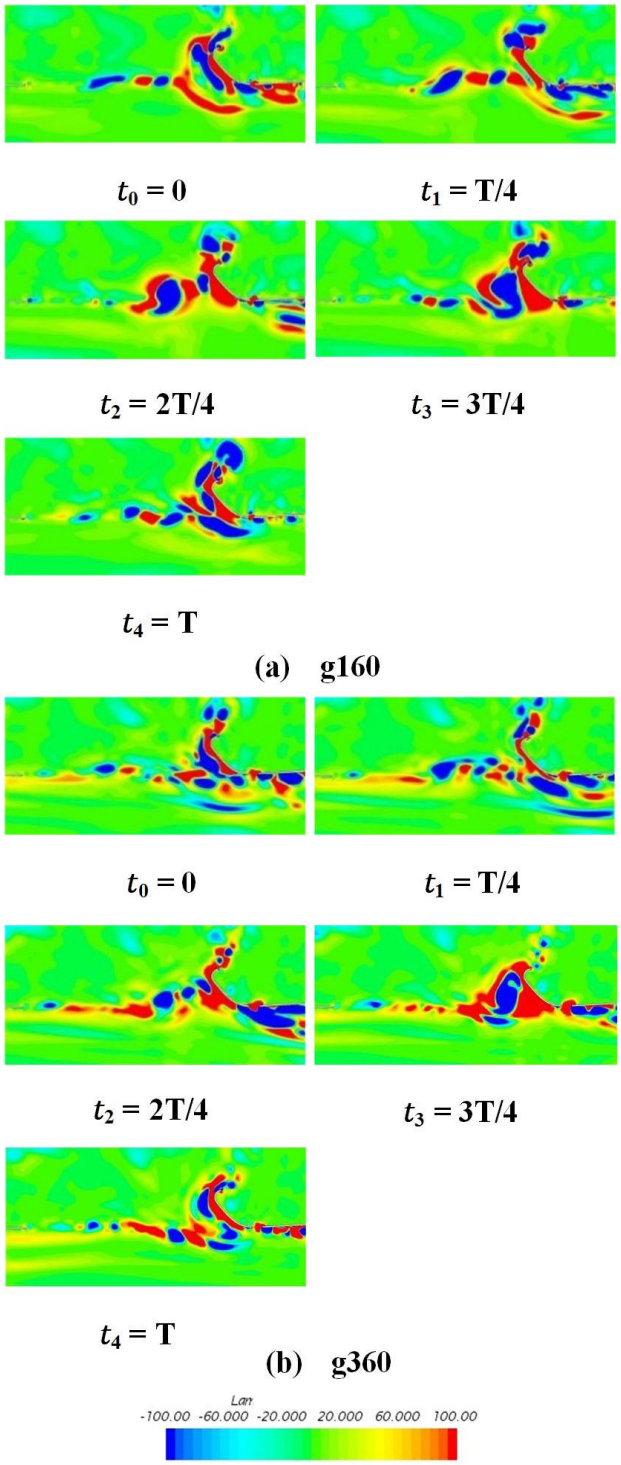

Fig. 11 Lambda 2 in the jet shear layer in a period

Cp_{rms} of g360 is lower than that of g160. The vortices in the jet shear layer of g360 are small and numerous. The fusion time of each vortex is delayed, and the fusion intensity is reduced.

Figure 12 presents the pressure of the base model and g360 in the XY plane. Compared with (a), the overall pressure fluctuation of g360 is significantly reduced and the throat gap alleviates the pressure accumulation and loss at the collector during the fluctuation period.

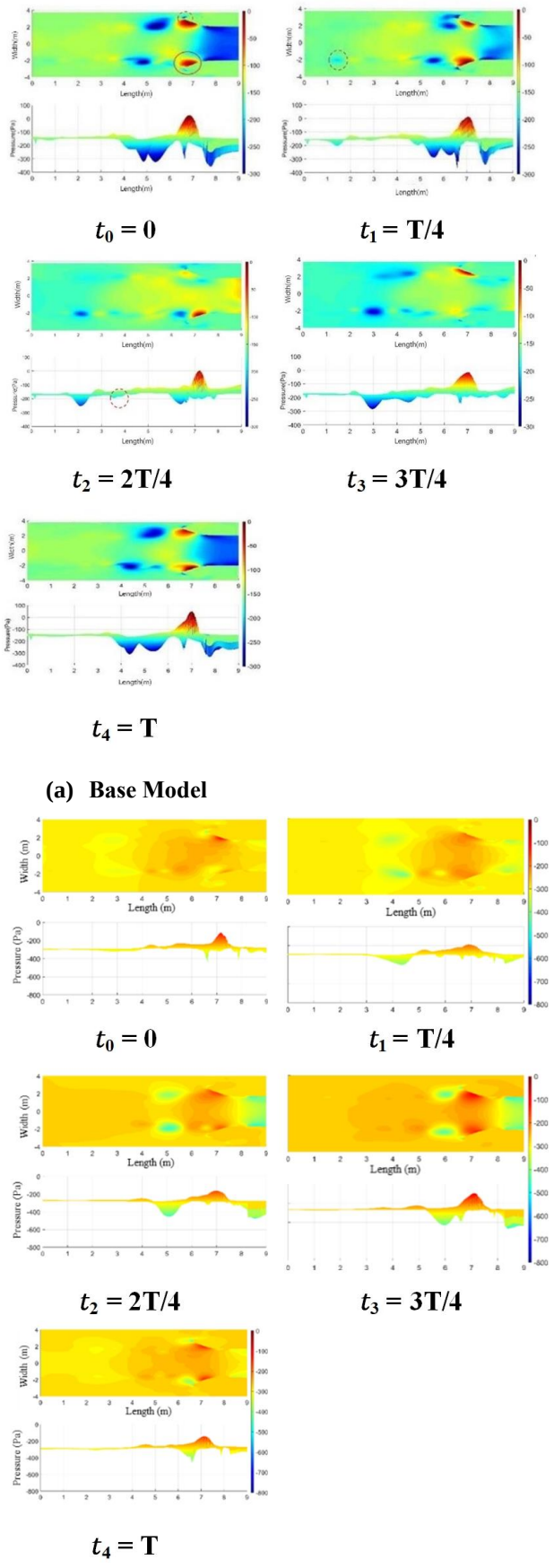

Fig. 12 Pressure in XY plane

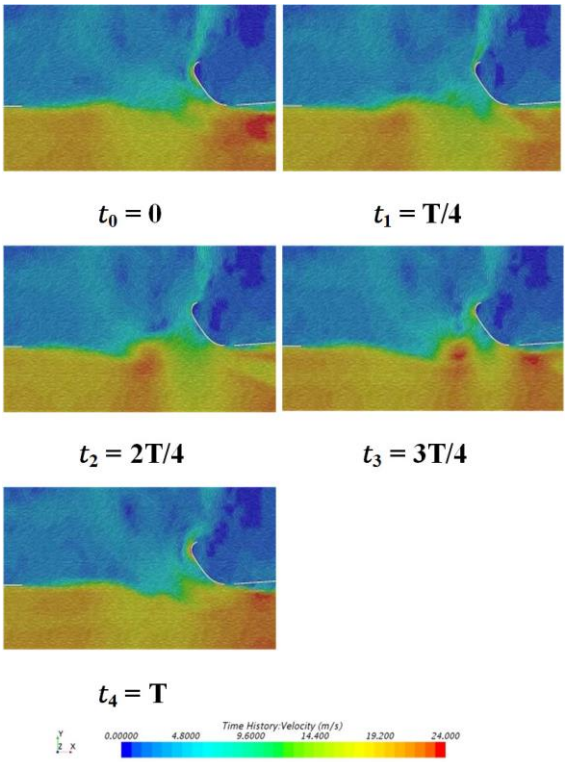

Fig. 13 Velocity vector in XY plane

Figure 13 illustrates the velocity vector in the XY plane of g360. The jet layer in the cycle still oscillates inside and outside. However, the amplitude is small. A comparison between Figs. 13 and 8 shows that the existence of the throat gap decreases the intensity of the air flow before and after the impact on the collector, and reduces the speed mutation area near the collector.

Figure 14 shows the flow field quality evaluation indicators under nine conditions. The air flow stability and the turbulence intensity at each position in the axial direction are stable with the increase of the gap length. This is due to the fact that when the gap length increases, the distance between the collector and the diffusion section gradually increases, which destroys the integrity of the circuit. Assuming that the length of the throat gap is infinite, only the collector remains in the flow field. This phenomenon is equivalent to the existence of barriers on the jet path in the free jet condition of the circular nozzle. At this time, a diffusion section is absent, and the pressure will not accumulate in a large amount. Pressure fluctuation will only be triggered when a circuit structure exists. The axial static pressure coefficient curve shows that when a throat gap exists, the static pressure coefficient fluctuation in the core area within 1–4 m can be alleviated.

4. Influence of External Contour of Collector on Pressure Fluctuation

The vortex generated at the nozzle exit is broken after hitting the collector, and the pressure wave generated during breaking exerts a certain impact on the newly generated vortex at the nozzle. In addition, the high

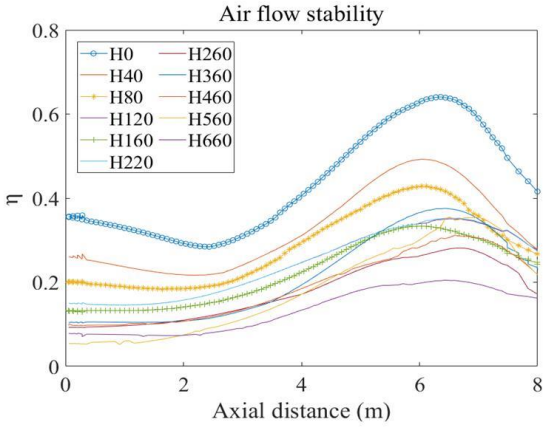

(a) Air flow stability

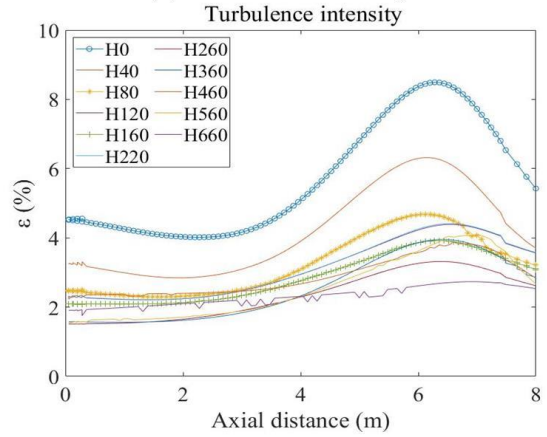

(b) Turbulence intensity

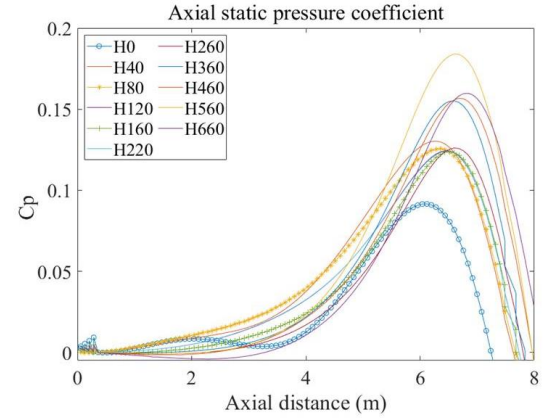

(c) Axial static pressure coefficient

Fig. 14 Quality evaluation indicators of the flow field

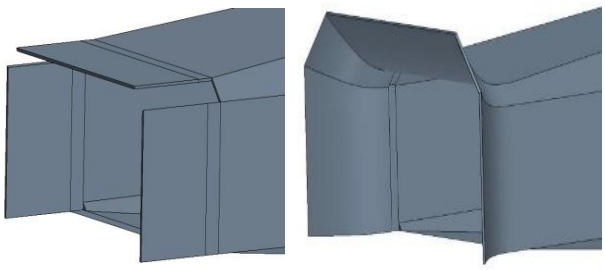

(a) Straight plate (b) Non-windward surface

Fig. 15 Shapes of the collector

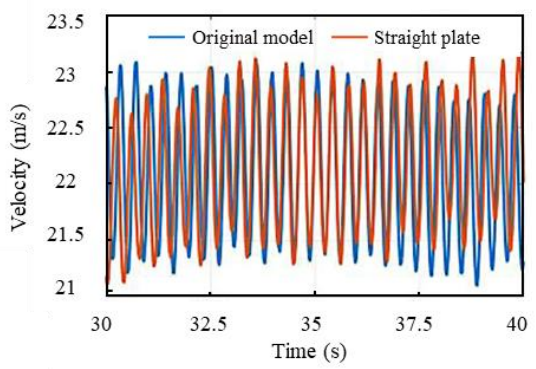

(a) Straight plate

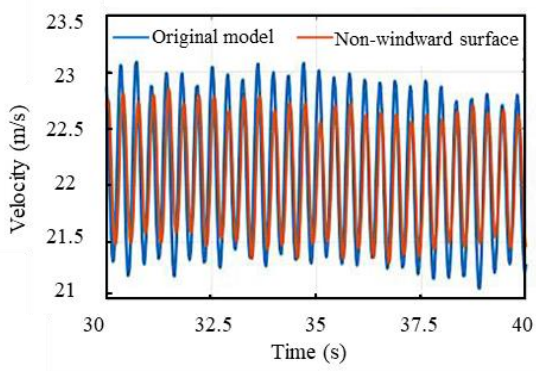

(b) Non-windward surface

Fig. 16 Time domain comparison

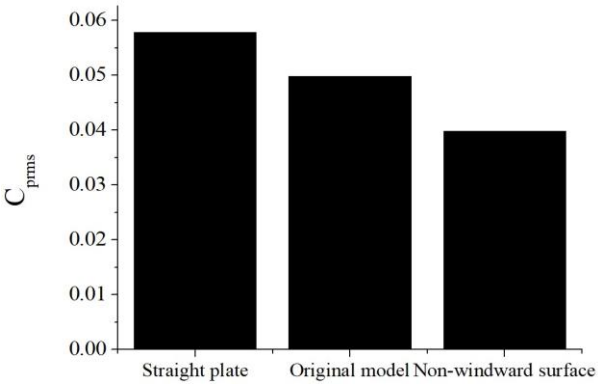

Fig. 17 Cp_{rms} of three conditions

pressure stored in the inner windward area of the collector and the continuous low pressure in the outer windward area result in the blockage of the flow field pressure. The influence of various baffles at the collector on the LFF is studied by changing the shape of the collector.

The collector exists as a source of vibration in the whole feedback. Two simple external contour models of the collector are first developed to investigate how the fluctuation phenomenon is impacted by the location and area of impact, given that the vortex structure directly affects the surface of the collector, as shown in Fig. 15.

Figure 16 shows a comparison of time domain between the two models and the original model. The amplitude of the velocity fluctuation of the straight plate is similar to that of the original model, and the mean value

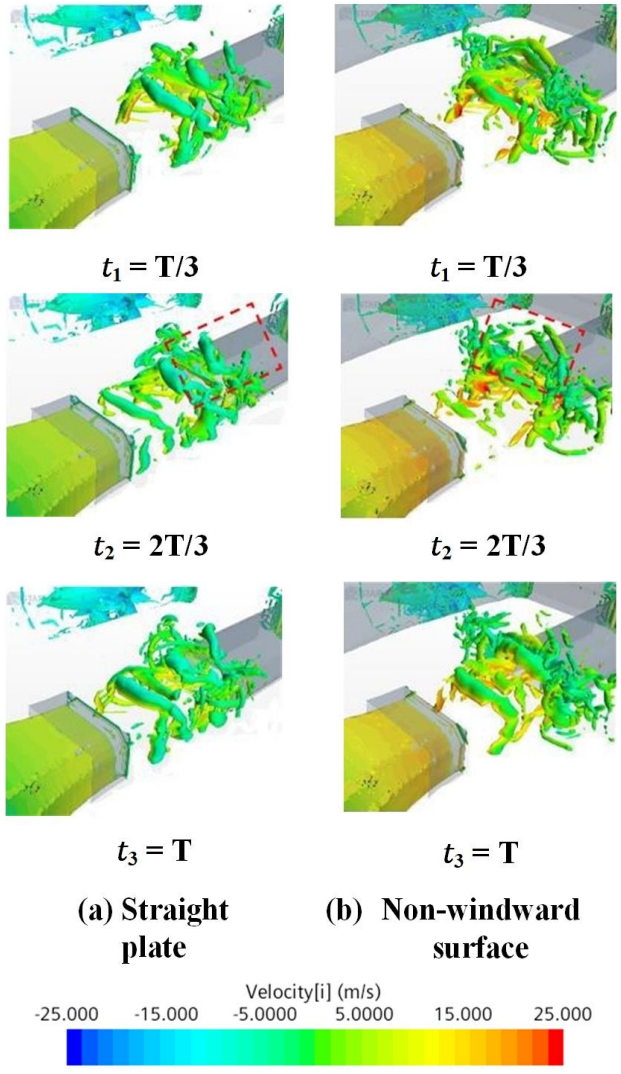

Fig 18. Iso-surface of Q criterion(Q=200/s²)

has a certain fluctuation. The reduction of the amplitude of the model velocity fluctuation without windward surface (Fig. 17) is reflected in the Cp_{rms}. That is, the straight plate model is slightly higher, and the model without windward surface is slightly lower.

Figure 18 illustrates vortex structures visualized by the iso-surfaces of the second invariant of the velocity gradient tensor $Q = 200 / s^2$ of the flow field domain, with two integral shapes for the period T_f. The vortex does not completely break after it collides with the collector in the straight plate scheme. The vortex ring continues to develop and break behind the outer of the test section in the marked area of Fig. 18 (a), which prolongs the duration of the pressure wave. The area of the vortex collision collector in the scheme without windward surface decreases and the broken vortex structure spreads in the YZ plane, as shown in the marked area of Fig. 18 (b). In addition, the higher vortex intensity of the straight plate scheme, compared with that of the non-windward surface, is reflected in the fluctuation phenomenon that the former is more serious than the latter.

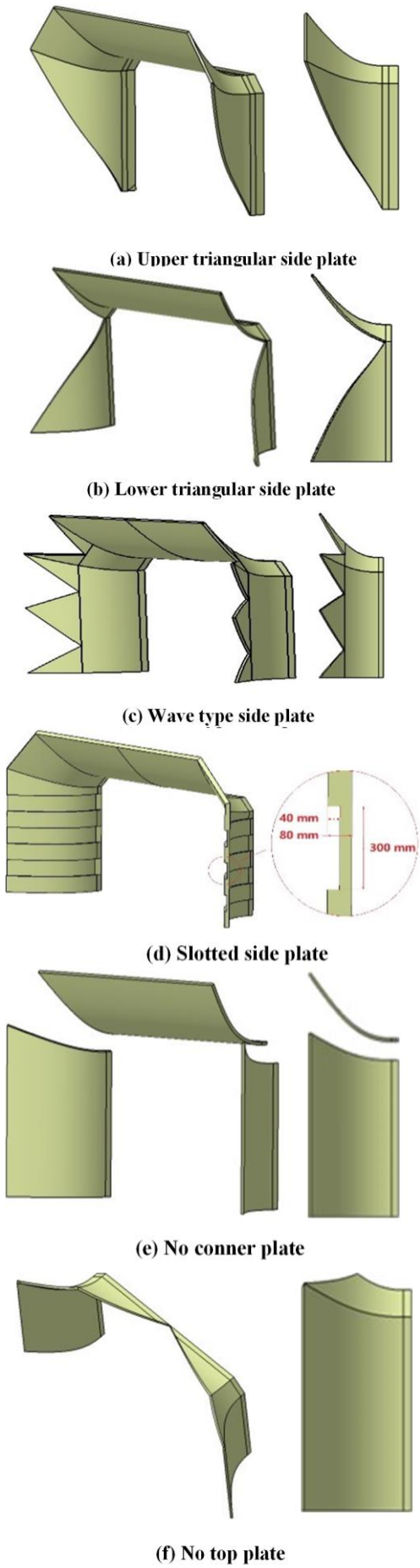

Fig. 19 Different modifications

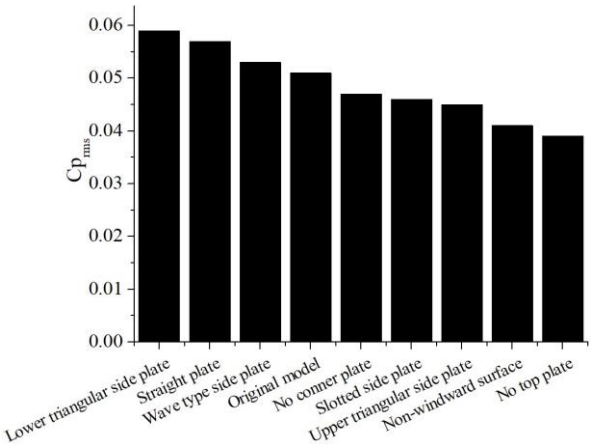

Fig. 20 Cp_{rms} of nine conditions

The model without windward surface presents a certain vibration reduction effect. The shape of the collectors of the models is further modified, and the side, corner, and top plates are subjected to different modifications (Fig. 19) to study the impact of the baffle shape on the pressure fluctuation. Option (a) keeps the top plate and corner plates unchanged, but an upper triangular side plate is used. Option (b) keeps the top plate unchanged, but retains the upper triangular part of the corner plate connected to the top plate and uses a lower triangular side plate connected to the floor plate. Option (c) keeps the top plate and corner plates the same as option (b), but uses a wave-type side plate. Option (d) keeps the top and corner plates unchanged, but uses a slotted structure for the side plates. The width of the slot is 300 mm and the depth is 40 mm. Option (e) keeps the top and side plates unchanged, but removes the corner plates. Option (f) keeps corner plates and side plates unchanged, but the top plate is V-shaped.

Figure 20 shows the Cp_{rms} of each modification scheme. The modification effect of the lower triangle of the side plate is the worst, and that of the upper triangle is slightly lower than that of the non-windward side. The optimal effect of the modification of the top plate indicates that the effect will become increasingly evident if the characteristic length of the continuous section increases. The following is a detailed discussion of several typical modification schemes.

Figure 21 shows the vortex structures visualized by the iso-surfaces of the second invariant of the velocity gradient tensor $Q = 200\ /s^2$ of the flow field domain with the side plate scheme for the period T_f. The moving speed of the top vortex in the flow field is slightly higher than that of the side, as shown in Fig. 21 (a). The delay in the contour of the lower triangular structure from bottom to top indicates that the vortex ring structure simultaneously affects the collector on three sides, which is more conducive to its breaking and causes pressure fluctuation. The contour and eddy current distribution trend of the upper triangular structure are opposite. Hence, the simultaneous impact of the vortex rings is avoided to some extent. However, the upper triangular structure demonstrates vortex whirling at the side plate

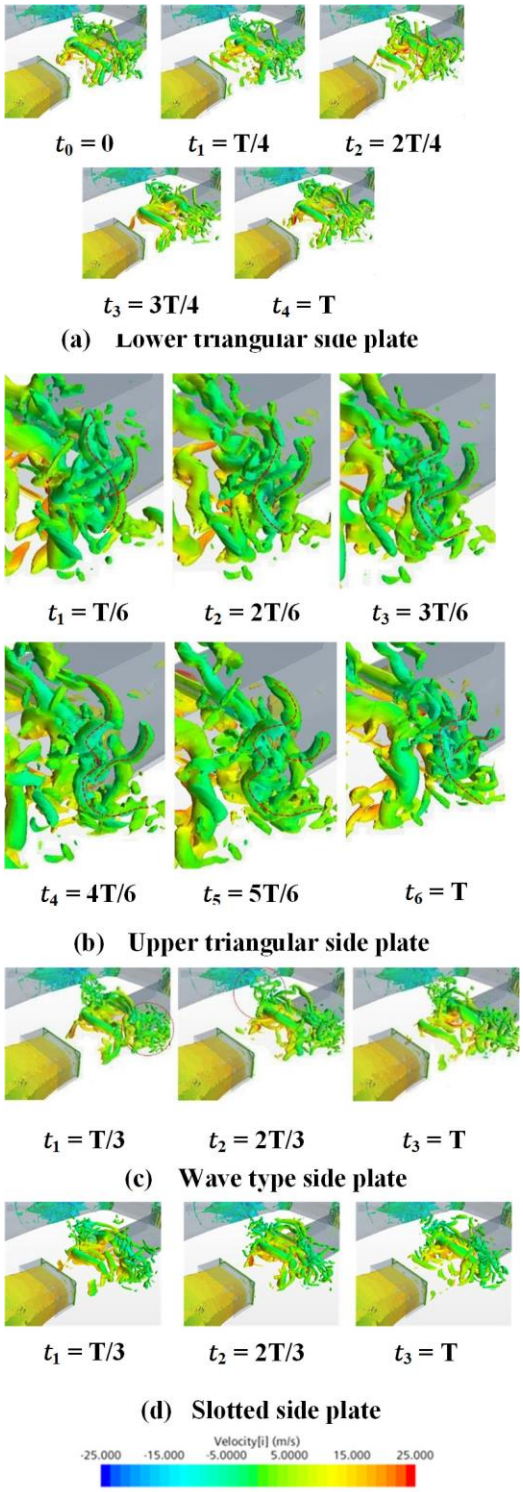

Fig. 21 Iso-surface of Q criterion of modification of side plates (Q=200 /s^2)

position, as shown in Fig. 18 (b). The vortex rotates clockwise when viewed from the top. The tornado-like structure prevents the broken vortex structure from spreading to the rear of the flow field, which is slightly distorted. It can be seen from Fig. 18 (c) that the wave-type structure only improves the uniformity of the broken vortex, while it does not affect the key areas of the flow field, and it slightly strengthens the fluctuation. It can be observed from Fig. 18 (d) that the vortex structure

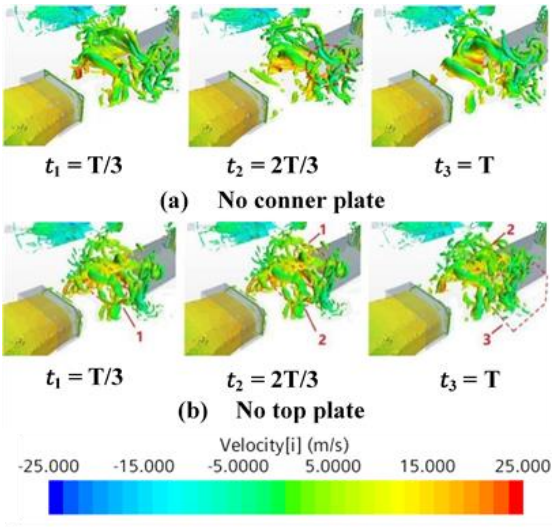

Fig. 22 Iso-surface of Q criterion of modification of top plates (Q=200 /s^2)

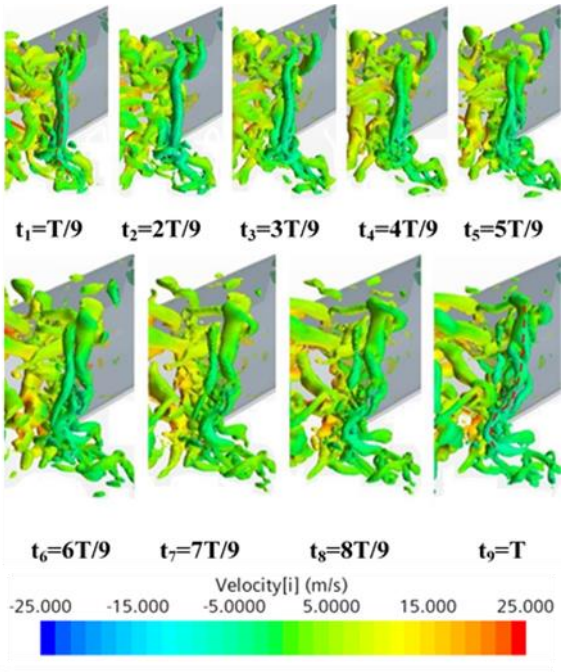

Fig. 23 Iso-surface of Q criterion of no top plates (Q=200 /s^2)

changing near the grooved structure staggers the time when the incoming flow impinges on different positions of the inner plate and exerts a certain diversion and buffering effect. However, this effect is unclear because its depth is limited by the thickness and size of the collector.

Figure 22 illustrates the vortex structures visualized by the iso-surfaces of the second invariant of the velocity gradient tensor $Q = 200 / s^2$ of the flow field domain without corner and top plate schemes for the period T_f. It can be seen from Fig. 22 (a) that the flow field change of the plate scheme without corner is unclear. Only the edge vortex of the side and top plates can easily pass

through the position of the corner plate with minimal impact on the fluctuation phenomenon. It can be observed from Fig. 22 (b) that the characteristic length in the width direction of the flow field without a top plate becomes smaller. This is due to the fact that the top of the collector is cut and the top vortex chain of the vortex ring 1 only partially hits the collector at $t2$, and part of it is directly released to the outer layer of the diffusion section, which weakens the energy of the pressure wave. In addition, the flow field near the side plate presents a tornado vortex structure in this scheme (Fig. 23). The whirling radius of the tornado vortex is small and increasingly three-dimensional because the shape of the side plate in this scheme remains intact. The escape of the broken vortex structure to the rear and side is minimal, and the energy intensifies in area 3 at moment $t3$ (Fig. 22 (b)), which may be due to the permanent presence of the vortex.

On the one hand, the vortex ring is subjected to its tangential force when it approaches the collector, which partially weakens and transforms the energy of the direct collision. On the other hand, it can absorb part of the energy of the pressure wave after the vortex is broken, to ensure that the scheme without the top plate can partially weaken the pressure fluctuation phenomenon. This phenomenon may be optimized to artificially generate a whirlpool and further reduce the pulsating pressure.

In summary, the following modification suggestions are put forward:

(1) The windward area of the collector is reduced to some extent, which indicates that the breakage of the vortex can be controlled to a certain extent and completely staggered, or a small amount of impact can be avoided.

(2) The time when the vortices hit the baffles at the collector can be staggered to reduce the number of vortices moving backward.

(3) The cyclonic vortex structure can be permanently located near the collector to alleviate the impact strength of the incoming vortex to a certain extent.

5. CONCLUSIONS

Essentially, in an open wind tunnel, LFFs can occur due to unstable vortices formed by the jet at the nozzle. This can lead to reduced accuracy in wind tunnel testing and decreased equipment lifespan. To address this issue, this study uses CFD methods to examine the causes and factors influencing LFF mechanisms in wind tunnels. The study also explores various techniques for reducing vibrations.

The pressure accumulation at the connection between the collector and the diffusion section was then relieved by increasing the length of the throat gap, and the pressure fluctuation phenomenon was reduced according to a certain rule. The relationship between the vibration reduction effect and the length of the gap was first proportional and then stepped, with a certain degree of mutation and stability.

The pressure feedback phenomenon can be reduced by changing the shape characteristics of the collector. The tail vortex ring seldom collided with the collector, the vortex structure continued to exist, and the pressure fluctuation phenomenon intensified when the collector was in a straight plate shape. The pressure fluctuation value can be reduced to a certain extent by appropriately reducing the windward surface area of the collector in order to control the breaking degree of the tail vortex ring. The comparison of the flow field of the upper and lower triangles demonstrated that the synchronism of the tail vortex affecting the baffles of the collector can affect the pressure fluctuation phenomenon. Some models can form a stationary tornado vortex structure at the tail of the test section to alleviate the vortex ring partially affecting the collector, and reduce the intensity of the pressure wave when breaking. The excitation frequency of the edge feedback effect remains unaffected by the modification schemes of these collectors. Although they fail to change the resonance phenomenon from the root, they still exert an actual cushioning effect.

CONFLICT OF INTEREST

HU Xingjun, LUO Yufei, SHI Keyuan, GUO Peng, and WANG Jingyu declare that they have no conflict of interest.

AUTHOR CONTRIBUTION

LUO Yufei wrote the manuscript and established the models. GUO Peng provided the concept and idea. SHI Keyuan and WANG Jingyu made suggestions to improve it. HU Xingjun provides of fund support.

Foundation item: Projects(2022YFE0208000) supported by the National Key R&D Program of China; Projects (GF-2022-03883) supported by Jilin Science and Technology Major Project.

REFERENCES

Abdelhamed, A. S., Yassen, Y. E. S., & ElSakka, M. M. (2014). Design optimization of three dimensional geometry of wind tunnel contraction. *Ain Shams Engineering Journal*, 6, 281-288. https://doi.org/10.1016/j.asej.2014.09.008.

Ahuja, K., Massey K., D'Agostino M., Ahuja, K., Massey, K., & D'Agostino, M. (1997). Flow/acoustic interactions in open-jet wind tunnels. *3rd AIAA/CEAS Aeroacoustics Conference*, 1691. https://doi.org/10.2514/6.1997-1691.

Amandolese, X., & Vartanian, C. (2010). Reduction of 3/4 open jet low-frequency fluctuations in the S2A wind tunnel. *Journal of Wind Engineering and Industrial Aerodynamics* 98(10), 568–574. https://doi.org/10.1016/j.jweia.2010.04.011.

Barlow, J. B., Rae, W. H., & Pope, A. (1999). *Low-Speed Wind Tunnel Testing*. Wiley.

Bender, T., Hoff, P., & Kleemann, R. (2011). The New BMW Climatic Testing Complex - The Energy and Environment Test Centre. *SAE Technical Paper* 2011-01-0167. https://doi.org/10.4271/2011-01-0167.

Blumrich, R., Widdecke, N., Wiedemann, J., Michelbach, A., Wittmeier, F., & Beland, O. (2015). New FKFS Technology at the Full-Scale Aeroacoustic Wind Tunnel of University of Stuttgart. *SAE Int J Passeng. Cars Mech Syst*, 8(1), 294–305. https://doi.org/10.4271/2015-01-1557.

Cabral, B., Leedom, L.C.(1993). Imaging Vector Fields Using Line Integral Convolution. *Proceedings of ACM SigGraph 93*, 27, 263-270. https://doi.org/10.1145/166117.166151.

Calautit, J.K., Hughes, B.R.(2016). CFD and experimental data of closed-loop wind tunnel flow. *Data in Brief*, 7(1), 216–220. https://doi.org/10.1016/j.dib.2016.02.033.

Doolan, C., Morgans, R. (2007). Numerical Evaluation and Optimization of Low Speed Wind Tunnel Contractions. *18th AIAA Computational Fluid Dynamics Conference*, Miami, Florida, United States.

Duell, E., Kharazi, A., Muller, S., & Ebeling, W. (2010). The BMW AVZ Wind Tunnel Center. *SAE 2010 World Congress & Exhibition*, 2010(01), 0118. https://doi.org/10.4271/2010-01-0118.

Duell, E. J., Yen, & Arnette, S.(2002). *Recent advances in large scale aeroacoustic wind tunnels*. 8th AIAA/CEAS Aeroacoustics Conference & Exhibit, Breckenridge, Colorado, United States. https://doi.org/10.2514/6.2002-2503.

Flandro, G. A. & Jacobs, H. R. (1973). "Vortex-generated Sound in Cavities,". *AIAA J.*, 973–1014, https://doi.org/10.2514/6.1973-1014.

Fu, L. (1998). *Automotive aerodynamics*. Machinery Industry Press, China.

Ghani, A, S.A.A, Aroussi, A., Rice, E.(2001). Simulation of road vehicle natural environment in a climatic wind tunnel. *Simulation Practice and Theory*, 8(6-7), 359-375. https://doi.org/10.1016/S0928-4869(00)00028-8

Gritskevich, M. S.,Garbaruk, A. V.,Schutze, J., Menter, F. R.(2012).Development of DDES and IDDES Formulations for the k-omega Shear Stress Transport Model. *Flow Turbulence And Combustion*, 88(3), 431-449. https://doi.org/10.1007/s10494-011-9378-4.

Holthusen, H., & Kooi, J. W.(1997). Model and full scale investigations of the low frequency vibration phenomena of the DNW open jet. *Tsentralni Aerogidrodinamicheskii Inst, AGARD conference proceedings*, 26, 1-26.

Hu, X., Luo, Y., Leng, J., Guo, P., Yu, T., & Wang, J.(2022). The low frequency pressure pulsation and control of the open-jet wind tunnel. *Scientific Reports* 12(1), 19090. https://doi.org/10.1038/s41598-022-22080-9.

Jia, Q., Zhu, Y., Bao, D., Rashidi, M. M., & Yang, Z. (2019). On the Low Frequency Pressure Fluctuation in a 3/4 Open Jet Automotive Wind Tunnel. *Journal of Applied Fluid Mechanics*, 12(5), 1359-1369. https://doi.org/10.29252/JAFM.12.05.29530.

Jin, L., Jiang, X., Liu, Z. & Deng, X. (2014). Study on the Effect and Mechanism of the Collecting Port Holes on the Low Frequency Oscillation in the FL-14 Wind Tunnel. *Abstracts of the 8th National Symposium on Fluid Mechanics*.

Kesharwani, S., Mistry, C. S., Roy, S., Roy, A., & Sinhamahapatra, K. P.(2017). Design aspects for large diameter, low speed axial flow fan for wind tunnel application. *Gas Turbine India Conference*, 58509. https://doi.org/10.1115/GTINDIA2017-4880

Kudo, T., Komatsu, Y., Maeda, K., & Nishimura, M. (2009). Techniques for Reducing Low-Frequency Fluctuations in Aeroacoustic Wind Tunnels. *Journal of Environment and Engineering* 4(2), 289–301. https://doi.org/10.1299/jee.4.289.

Lacey, J. (2004). Concept for reducing the cost of subsonic wind tunnels. *AIAA Paper* No. 2004-6828, *USAF Developmental Test and Evaluation Summit*. https://doi.org/10.2514/6.2004-6828.

Li, Q., Yang, F., & Yang, Z. (2009). Application and Comparison of Two Turbulence Models in Calculation of Wind Tunnel Corner Flow Field. *Computer Aided Engineering*, 18(1), 38-42. https://doi.org/10.3969/j.issn.1006-0871.2009.01.010

Li, Q., Chen, L., Yang, Z., & Xu, Y. (2014). Axial static pressure coefficient of automotive wind tunnel test section at different diffusion angles. *Journal of Tongji University (Natural Science Edition)*, 42(8),1227. https://doi.org/10.3969/j.issn.0253-374x.2014.08.013

Li, Q., Dai, W., Du, K., & Yang, Z. (2017). Influence of Wind Tunnel Structure on Static Pressure Coefficient and Gradient in Test Section. *Journal of Tongji University (Natural Science Edition)*, 45(10),1506-1511. https://doi.org/10.11908/j.issn.0253-374x.2017.10.013

Li, Q., Zheng, Z., Jia, Q., & Yang, Z. (2010). Two Methods for Improving the Axial Static Pressure Coefficient of Automotive Wind Tunnel. *Journal of Tongji University (Natural Science Edition)*. https://doi.org/10.3969/j.issn.0253-374x.2010.03.020

Li, Z.(2015). Wind Tunnel Test Manual. *Aviation Industry Press*.

Liu, Z. (2005). Structural design of wind tunnel. *China Astronautic Publishing House*.

Manuel, G.S.(1992). Effect of collector fonfiguration on test section turbulence levels in an open-jet wind tunnel. *NASA, Scientific and Technical Information Program*.

Menter,F. R., & Kuntz, M. (2004). Adaptation of Eddy-Viscosity Turbulence Models to Unsteady Separated Flow Behind Vehicles. *The Aerodynamics of Heavy Vehicles: Trucks, Buses, and Trains*, 339–352. https://doi.org/10.1007/978-3-540-44419-0_30.

Nikitin, N. V., & Nicoud, F. (2000). An approach to wall modeling in large-eddy simulations. *Physics of Fluids*, 12(7), 1629-1632. https://doi.org/10.1063/1.870414

Owen, F. K. , & Owen, A. K.(2008). Measurement and assessment of wind tunnel flow quality. *Progress in Aerospace Sciences* 44(5), 315–348. https://doi.org/10.1016/j.paerosci.2008.04.002.

Qu, X. L., Zhao, F., Song, B. B., Wang, X. L.,Yu, & Y. S. (2018). *Experimental study on suppression of low frequency pressure pulsation in open test section of large low speed wind tunnel*. *Abstracts of the 10th National Conference on fluid mechanics*, China.

Rennie, M., Kim, M. S., Lee, J. H., Kee, J. D. (2004). Suppression of Open-Jet Pressure Fluctuations in the Hyundai Aeroacoustic Wind Tunnel. *SAE 2004 World Congress & Exhibition*, 2004(01), 0803. https://doi.org/10.4271/2004- 01-0803.

Reshotko, E., Saric, W., & Nagib, H.(1997). Flow quality issues for large wind tunnels. *35th Aerospace Sciences Meeting and Exhibit*, 225. https://doi.org/10.2514/6.1997-225.

Saric, W., & Reshotko, E.(1998). Review of flow quality issues in wind tunnel testing. *20th AIAA Advanced Measurement and Ground Testing Technology Conference. American Institute of Aeronautics and Astronautics Inc, AIAA*. https://doi.org/10.2514/6.1998-2613.

Sellers, I., Applin, W. L.Z. T., Molloy, J. K., & Gentry, G. L. L.(1985). Effect of jet exit vanes on flow pulsations in an open-jet wind tunnel. *NASA Technical Memorandum.*

Soderman, P. T., & Olson, L. E.(1992). The design of test-section inserts for higher speed aeroacoustic testing in the Ames 80-by 120-foot wind tunnel. *DGLR/AIAA 14th Aeroacoustics Conference*.

Tadakuma, K., Sugiyama, T., Maeda, K., Iyota, M., Ohta, M., & Komatsu, Y.(2014). Development of Full-Scale Wind Tunnel for Enhancement of Vehicle Aerodynamic and Aero-Acoustic Performance. *SAE International Journal of Passenger Cars - Mechanical Systems* 7(2) ,603–616. https://doi.org/10.4271/2014-01-0598.

Taketo, T. (1989). Automotive aerodynamics. *Jilin Science and Technology Press*.

Thomas, S. (2016). Aerodynamics of Road Vehicle. *SAE International*.

Walter, J., Duell, E., Martindale, B., Arnette, & S.,Geierman, R.(2003). The Daimler Chrysler full scale aeroacoustic wind tunnel. *SAE Transactions*, 112, 324–340. https://doi.org/10.2307/44745404

Wiedemann, J., Wickern, G., Ewald, B., & Mattern, C. (1993). Audi Aero-Acoustic Wind Tunnel. *SAE Technical Paper 930300* 1–16. https://doi.org/10.4271/930300.

Xu, Y., Yang, Z., & Li, Q .(2014). Effect of the shape and angle of the collecting port on the axial static pressure factor of the automotive wind tunnel test section. *Computer Aided Engineering*, 23(4), 12-16. https://doi.org/ 10.13340/j.cae.2014.04.003

Yang, Z., & Zhao, L. (2017). *Effect of solidity on wind tunnel corner vane losses.* The 5th International Conference on Nonlinear Mechanics. Shanghai University, 1180-1186.

Zanoun, E. S. (2018). Flow characteristics in low-speed wind tunnel contractions: Simulation and testing. *Alexandria Engineering Journal*, 57(4), 2265–2277. https://doi.org/10.1016/j.aej.2017.08.024.

Zheng, Z. Q., Wang, Y. G., & Yang, Z. G. (2007). An experimental study on the suppression of the low-frequency pulsation of model wind tunnel. *Automotive Engineering* 5, 369-372. https://doi.org/ 10.19562/j.chinasae.qcgc.2007.05.002